

## 2

# Atomic Collisions and Backscattering Spectrometry

## 2.1 Introduction

The model of the atom is that of a cloud of electrons surrounding a positively charged central core—the nucleus—that contains  $Z$  protons and  $A - Z$  neutrons, where  $Z$  is the atomic number and  $A$  the mass number. Single-collision, large-angle scattering of alpha particles by the positively charged nucleus not only established this model but also forms the basis for one modern analytical technique, Rutherford backscattering spectrometry. In this chapter, we will develop the physical concepts underlying Coulomb scattering of a fast light ion by a more massive stationary atom.

Of all the analytical techniques, Rutherford backscattering spectrometry is perhaps the easiest to understand and to apply because it is based on classical scattering in a central-force field. Aside from the accelerator, which provides a collimated beam of MeV particles (usually  $^4\text{He}^+$  ions), the instrumentation is simple (Fig. 2.1a). Semiconductor nuclear particle detectors are used that have an output voltage pulse proportional to the energy of the particles scattered from the sample into the detector. The technique is also the most quantitative, as MeV He ions undergo close-impact scattering collisions that are governed by the well-known Coulomb repulsion between the positively charged nuclei of the projectile and target atom. The kinematics of the collision and the scattering cross section are independent of chemical bonding, and hence backscattering measurements are insensitive to electronic configuration or chemical bonding with the target. To obtain information on the electronic configuration, one must employ analytical techniques such as photoelectron spectroscopy that rely on transitions in the electron shells.

In this chapter, we treat scattering between two positively charged bodies of atomic numbers  $Z_1$  and  $Z_2$ . The convention is to use the subscript 1 to denote the incident particle and the subscript 2 to denote the target atom. We first consider energy transfers during collisions, as they provide the identity of the target atom. Then we calculate the scattering cross section, which is the basis of the quantitative aspect of Rutherford backscattering. Here we are concerned with scattering from atoms on the sample surface or from thin layers. In Chapter 3, we discuss depth profiles.

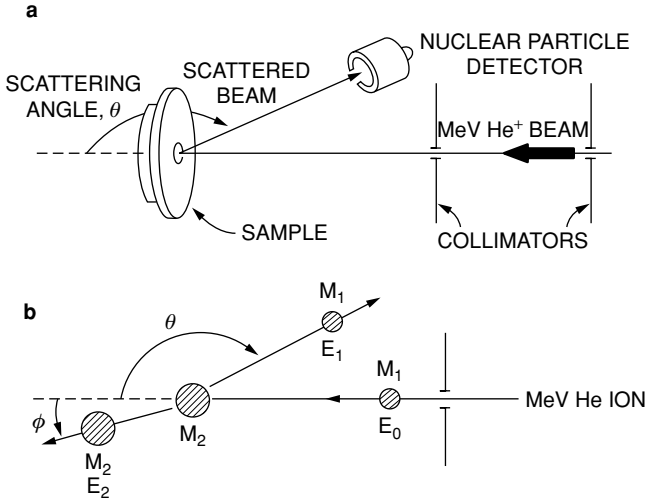


FIGURE 2.1. Nuclear particle detector with respect to scattering angle courtesy of MeV He<sup>+</sup> electron beam.

## 2.2 Kinematics of Elastic Collisions

In Rutherford backscattering spectrometry, monoenergetic particles in the incident beam collide with target atoms and are scattered backwards into the detector-analysis system, which measures the energies of the particles. In the collision, energy is transferred from the moving particle to the stationary target atom; the reduction in energy of the scattered particle depends on the masses of incident and target atoms and provides the signature of the target atoms.

The energy transfers or kinematics in elastic collisions between two isolated particles can be solved fully by applying the principles of conservation of energy and momentum. For an incident energetic particle of mass  $M_1$ , the values of the velocity and energy are  $v$  and  $E_0(=1/2 M_1 v^2)$ , while the target atom of mass  $M_2$  is at rest. After the collision, the values of the velocities  $v_1$  and  $v_2$  and energies  $E_1$  and  $E_2$  of the projectile and target atoms are determined by the scattering angle  $\theta$  and recoil angle  $\phi$ . The notation and geometry for the laboratory system of coordinates are given in Fig. 2.1b.

Conservation of energy and conservation of momentum parallel and perpendicular to the direction of incidence are expressed by the equations

$$\frac{1}{2} M_1 v^2 = \frac{1}{2} M_1 v_1^2 + \frac{1}{2} M_2 v_2^2, \quad (2.1)$$

$$M_1 v = M_1 v_1 \cos \theta + M_2 v_2 \cos \phi, \quad (2.2)$$

$$0 = M_1 v_1 \sin \theta - M_2 v_2 \sin \phi. \quad (2.3)$$

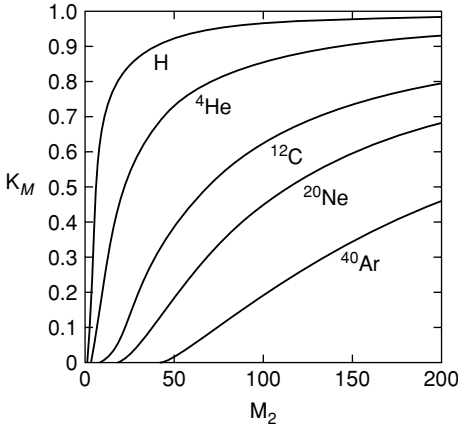


FIGURE 2.2. Representation of the kinematic factor  $K_{M_2}$  (Eq. 2.5) for scattering angle  $\theta = 170^\circ$  as a function of the target mass  $M_2$  for  $^1\text{H}$ ,  $^4\text{He}^+$ ,  $^{12}\text{C}$ ,  $^{20}\text{Ne}$ , and  $^{40}\text{Ar}$ .

Eliminating  $\phi$  first and then  $v_2$ , one finds the ratio of particle velocities:

$$\frac{v_1}{v} = \left[ \frac{\pm(M_2^2 - M_1^2 \sin^2 \theta)^{1/2} + M_1 \cos \theta}{M_2 + M_1} \right]. \quad (2.4)$$

The ratio of the projectile energies for  $M_1 < M_2$ , where the plus sign holds, is

$$\frac{E_1}{E_0} = \left[ \frac{(M_2^2 - M_1^2 \sin^2 \theta)^{1/2} + M_1 \cos \theta}{M_2 + M_1} \right]^2. \quad (2.5)$$

The energy ratio, called the *kinematic factor*  $K = E_1/E_0$ , shows that the energy after scattering is determined only by the masses of the particle and target atom and the scattering angle. A subscript is usually added to  $K$ , i.e.,  $K_{M_2}$ , to indicate the target atom mass. Tabulations of  $K$  values for different  $M_2$  and  $\theta$  values are given in Appendix 1 and are shown in Fig. 2.2 for  $\theta = 170^\circ$ . Such tables and figures are used routinely in the design of backscattering experiments. A summary of scattering relations is given in Table 3.1.

For direct backscattering through  $180^\circ$ , the energy ratio has its lowest value given by

$$\frac{E_1}{E_0} = \left( \frac{M_2 - M_1}{M_2 + M_1} \right)^2 \quad (2.6a)$$

and at  $90^\circ$  given by

$$\frac{E_1}{E_0} = \frac{M_2 - M_1}{M_2 + M_1}. \quad (2.6b)$$

In collisions where  $M_1 = M_2$ , the incident particle is at rest after the collision, with all the energy transferred to the target atom, a feature well known in billiards. For  $\theta = 180^\circ$ , the energy  $E_2$  transferred to the target atom has its maximum value given by

$$\frac{E_2}{E_0} = \frac{4M_1 M_2}{(M_1 + M_2)^2}, \quad (2.7)$$

with the general relation given by

$$\frac{E_2}{E_0} = \frac{4M_1 M_2}{(M_1 + M_2)^2} \cos^2 \phi. \quad (2.7')$$

In practice, when a target contains two types of atoms that differ in their masses by a small amount  $\Delta M_2$ , the experimental geometry is adjusted to produce as large a change  $\Delta E_1$  as possible in the measured energy  $E_1$  of the projectile after the collision. A change of  $\Delta M_2$  (for fixed  $M_1 < M_2$ ) gives the largest change of  $K$  when  $\theta = 180^\circ$ . Thus  $\theta = 180^\circ$  is the preferred location for the detector ( $\theta \cong 170^\circ$  in practice because of detector size), an experimental arrangement that has given the method its name of *backscattering spectrometry*.

The ability to distinguish between two types of target atoms that differ in their masses by a small amount  $\Delta M_2$  is determined by the ability of the experimental energy measurement system to resolve small differences  $\Delta E_1$  in the energies of backscattered particles. Most MeV  $^4\text{He}^+$  backscattering apparatuses use a surface-barrier solid-state nuclear-particle detector for measurement of the energy spectrum of the backscattered particles. As shown in Fig. 2.3, the nuclear particle detector operates by the collection of the hole–electron pairs created by the incident particle in the depletion region of the reverse-biased Schottky barrier diode. The statistical fluctuations in the number of electron–hole pairs produce a spread in the output signal resulting in a finite resolution.

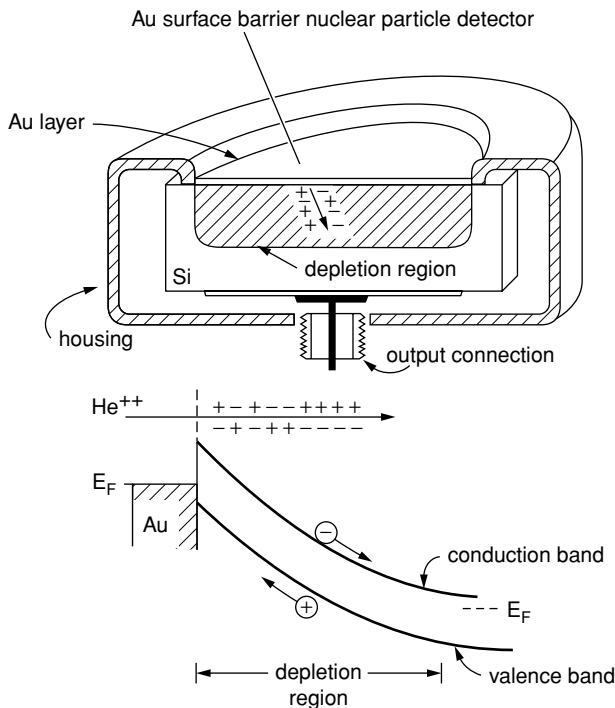


FIGURE 2.3. Schematic diagram of the operation of a gold surface barrier nuclear particle detector. The upper portion of the figure shows a cutaway sketch of silicon with gold film mounted in the detector housing. The lower portion shows an alpha particle, the  $\text{He}^+$  ion, forming holes and electrons over the penetration path. The energy-band diagram of a reverse biased detector (positive polarity on  $n$ -type silicon) shows the electrons and holes swept apart by the high electric field within the depletion region.

Energy resolution values of 10–20 keV, full width at half maximum (FWHM), for MeV  ${}^4\text{He}^+$  ions can be obtained with conventional electronic systems. For example, backscattering analysis with 2.0 MeV  ${}^4\text{He}^+$  particles can resolve isotopes up to about mass 40 (the chlorine isotopes, for example). Around target masses close to 200, the mass resolution is about 20, which means that one cannot distinguish among atoms between  ${}^{181}\text{Ta}$  and  ${}^{201}\text{Hg}$ .

In backscattering measurements, the signals from the semiconductor detector electronic system are in the form of voltage pulses. The heights of the pulses are proportional to the incident energy of the particles. The pulse height analyzer stores pulses of a given height in a given voltage bin or channel (hence the alternate description, *multichannel analyzer*). The channel numbers are calibrated in terms of the pulse height, and hence there is a direct relationship between channel number and energy.

### 2.3 Rutherford Backscattering Spectrometry

In backscattering spectrometry, the mass differences of different elements and isotopes can be distinguished. Figure 2.4 shows a backscattering spectrum from a sample with approximately one monolayer of  ${}^{63,65}\text{Cu}$ ,  ${}^{107,109}\text{Ag}$ , and  ${}^{197}\text{Au}$ . The various elements are well separated in the spectrum and easily identified. Absolute coverages can be determined from knowledge of the absolute cross section discussed in the following section. The spectrum is an illustration of the fact that heavy elements on a light substrate can be investigated at coverages well below a monolayer.

The limits of the mass resolution are indicated by the peak separation of the various isotopes. In Fig. 2.4, the different isotopic masses of  ${}^{63}\text{Cu}$  and  ${}^{65}\text{Cu}$ , which have a natural abundance of 69% and 31%, respectively, have values of the energy ratio, or kinematic factor  $K$ , of 0.777 and 0.783 for  $\theta = 170^\circ$  and incident  ${}^4\text{He}^+$  ions ( $M_1 = 4$ ).

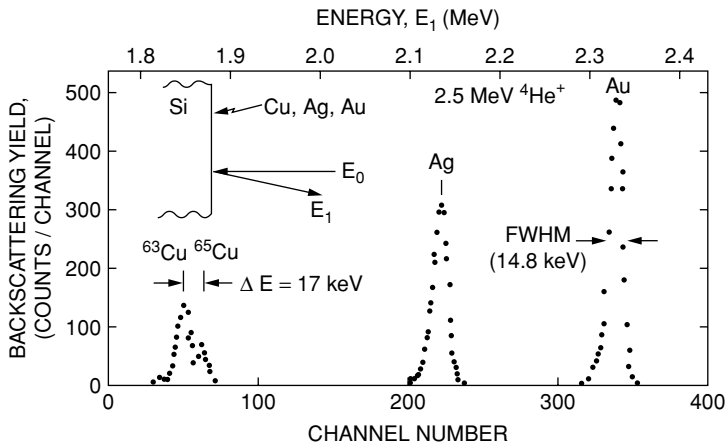


FIGURE 2.4. Backscattering spectrum for  $\theta = 170^\circ$  and 2.5 MeV  ${}^4\text{He}^+$  ions incident on a target with approximately one monolayer coverage of Cu, Ag, and Au. The spectrum is displayed as raw data from a multichannel analyzer, i.e., in counts/channel and channel number.

For incident energies of 2.5 MeV, the energy difference of particles from the two masses is 17 keV, an energy value close to the energy resolution (FWHM = 14.8 keV) of the semiconductor particle-detector system. Consequently, the signals from the two isotopes overlap to produce the peak and shoulder shown in the figure. Particles scattered from the two Ag isotopes,  $^{107}\text{Ag}$  and  $^{109}\text{Ag}$ , have too small an energy difference, 6 keV, and hence the signal from Ag appears as a single peak.

## 2.4 Scattering Cross Section and Impact Parameter

The identity of target atoms is established by the energy of the scattered particle after an elastic collision. The number  $N_s$  of target atoms per unit area is determined by the probability of a collision between the incident particles and target atoms as measured by the total number  $Q_D$  of detected particles for a given number  $Q$  of particles incident on the target in the geometry shown in Fig. 2.5. The connection between the number of target atoms  $N_s$  and detected particles is given by the scattering cross section. For a thin target of thickness  $t$  with  $N$  atoms/cm<sup>3</sup>,  $N_s = Nt$ .

The differential scattering cross section,  $d\sigma/d\Omega$ , of a target atom for scattering an incident particle through an angle  $\theta$  into a differential solid angle  $d\Omega$  centered about  $\theta$  is given by

$$\frac{d\sigma(\theta)}{d\Omega} d\Omega \cdot N_s = \frac{\text{Number of particles scattered into } d\Omega}{\text{Total number of incident particles}}.$$

In backscattering spectrometry, the detector solid angle  $\Omega$  is small ( $10^{-2}$  steradian or less), so that one defines an average differential scattering cross section  $\sigma(\theta)$ ,

$$\sigma(\theta) = \frac{1}{\Omega} \int_{\Omega} \frac{d\sigma}{d\Omega} \cdot d\Omega, \quad (2.8)$$

where  $\sigma(\theta)$  is usually called the *scattering cross section*. For a small detector of area  $A$ , at distance  $l$  from the target, the solid angle is given by  $A/l^2$  in steradians. For the geometry of Fig. 2.5, the number  $N_s$  of target atoms/cm<sup>2</sup> is related to the yield  $Y$  or the number  $Q_D$  of detected particles (in an ideal, 100%-efficient detector that subtends a solid angle  $\Omega$ ) by

$$Y = Q_D = \sigma(\theta)\Omega Q N_s, \quad (2.9)$$

where  $Q$  is the total number of incident particles in the beam. The value of  $Q$  is

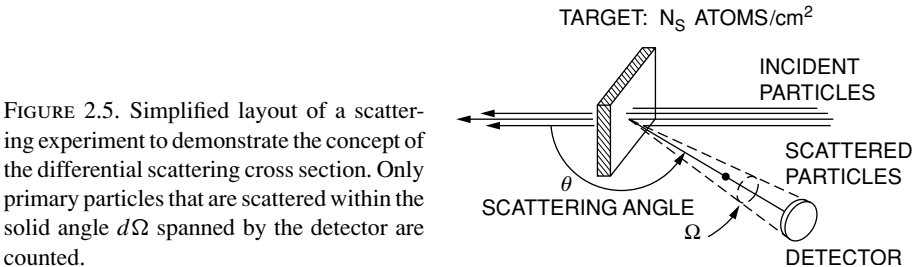


FIGURE 2.5. Simplified layout of a scattering experiment to demonstrate the concept of the differential scattering cross section. Only primary particles that are scattered within the solid angle  $d\Omega$  spanned by the detector are counted.

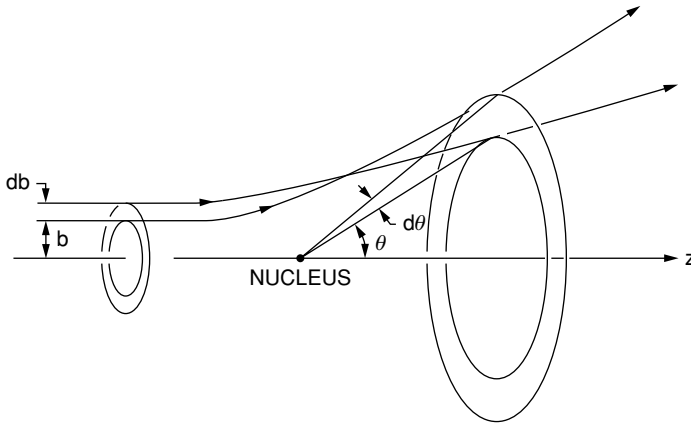


FIGURE 2.6. Schematic illustrating the number of particles between  $b$  and  $b + db$  being deflected into an angular region  $2\pi \sin \theta d\theta$ . The cross section is, by definition, the proportionality constant;  $2\pi b db = -\sigma(\theta)2\pi \sin \theta d\theta$ .

determined by the time integration of the current of charged particles incident on the target. From Eq. 2.9, one can also note that the name *cross section* is appropriate in that  $\sigma(\theta)$  has the dimensions of an area.

The scattering cross section can be calculated from the force that acts during the collision between the projectile and target atom. For most cases in backscattering spectrometry, the distance of closest approach during the collision is well within the electron orbit, so the force can be described as an unscreened Coulomb repulsion of two positively charged nuclei, with charge given by the atomic numbers  $Z_1$  and  $Z_2$  of the projectile and target atoms. We derive this unscreened scattering cross section in Section 2.5 and treat the small correction due to electron screening in Section 2.7.

The deflection of the particles in a one-body formulation is treated as the scattering of particles by a center of force in which the kinetic energy of the particle is conserved. As shown in Fig. 2.6, we can define the impact parameter  $b$  as the perpendicular distance between the incident particle path and the parallel line through the target nucleus. Particles incident with impact parameters between  $b$  and  $b + db$  will be scattered through angles between  $\theta$  and  $\theta + d\theta$ . With central forces, there must be complete symmetry around the axis of the beam so that

$$2\pi b db = -\sigma(\theta) 2\pi \sin \theta d\theta. \quad (2.10)$$

In this case, the scattering cross section  $\sigma(\theta)$  relates the initial uniform distribution of impact parameters to the outgoing angular distribution. The minus sign indicates that an increase in the impact parameter results in less force on the particle so that there is a decrease in the scattering angle.

## 2.5 Central Force Scattering

The scattering cross section for central force scattering can be calculated for small deflections from the impulse imparted to the particle as it passes the target atom. As

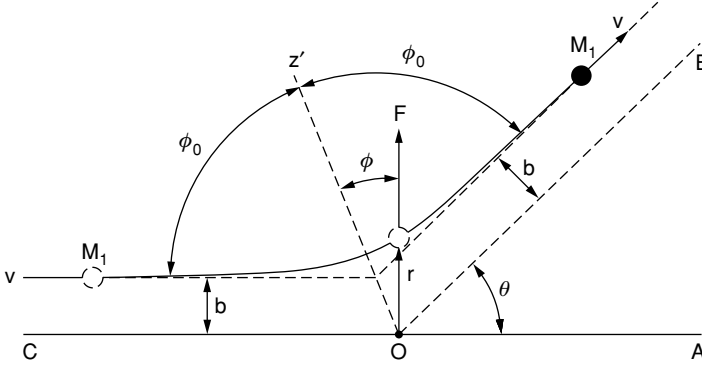


FIGURE 2.7. Rutherford scattering geometry. The nucleus is assumed to be a point charge at the origin  $O$ . At any distance  $r$ , the particle experiences a repulsive force. The particle travels along a hyperbolic path that is initially parallel to line  $OA$  a distance  $b$  from it and finally parallel to line  $OB$ , which makes an angle  $\theta$  with  $OA$ . The scattering angle  $\theta$  can be related to impact parameter  $b$  by classical mechanics.

the particle with charge  $Z_1e$  approaches the target atom, charge  $Z_2e$ , it will experience a repulsive force that will cause its trajectory to deviate from the incident straight line path (Fig. 2.7). The value of the Coulomb force  $F$  at a distance  $r$  is given by

$$F = \frac{Z_1 Z_2 e^2}{r^2}. \quad (2.11)$$

Let  $\mathbf{p}_1$  and  $\mathbf{p}_2$  be the initial and final momentum vectors of the particle. From Fig. 2.8, it is evident that the total change in momentum  $\Delta \mathbf{p} = \mathbf{p}_2 - \mathbf{p}_1$  is along the  $z'$  axis. In this calculation, the magnitude of the momentum does not change. From the isosceles triangle formed by  $\mathbf{p}_1$ ,  $\mathbf{p}_2$ , and  $\Delta \mathbf{p}$  shown in Fig. 2.8, we have

$$\frac{\frac{1}{2} \Delta p}{M_1 v} = \sin \frac{\theta}{2}$$

or

$$\Delta p = 2M_1 v \sin \frac{\theta}{2}. \quad (2.12)$$

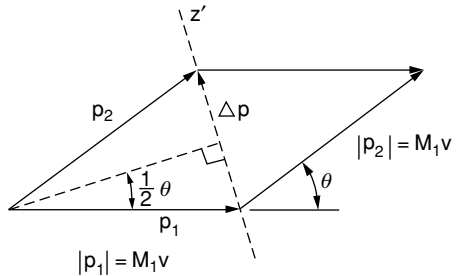


FIGURE 2.8. Momentum diagram for Rutherford scattering. Note that  $|\mathbf{p}_1| = |\mathbf{p}_2|$ , i.e., for elastic scattering the energy and the speed of the projectile are the same before and after the collision.



We now write Newton's law for the particle,  $\mathbf{F} = d\mathbf{p}/dt$ , or

$$d\mathbf{p} = \mathbf{F} dt.$$

The force  $F$  is given by Coulomb's law and is in the radial direction. Taking components along the  $z'$  direction, and integrating to obtain  $\Delta p$ , we have

$$\Delta p = \int (dp)_{z'} = \int F \cos \phi dt = \int F \cos \phi \frac{dt}{d\phi} d\phi, \quad (2.13)$$

where we have changed the variable of integration from  $t$  to the angle  $\phi$ . We can relate  $dt/d\phi$  to the angular momentum of the particle about the origin. Since the force is central (i.e., acts along the line joining the particle and the nucleus at the origin), there is no torque about the origin, and the angular momentum of the particle is conserved. Initially, the angular momentum has the magnitude  $M_1 v b$ . At a later time, it is  $M_1 r^2 d\phi/dt$ . Conservation of angular momentum thus gives

$$M_1 r^2 \frac{d\phi}{dt} = M_1 v b$$

or

$$\frac{dt}{d\phi} = \frac{r^2}{vb}.$$

Substituting this result and Eq. 2.11 for the force in Eq. 2.13, we obtain

$$\Delta p = \frac{Z_1 Z_2 e^2}{r^2} \int \cos \phi \frac{r^2}{vb} d\phi = \frac{Z_1 Z_2 e^2}{vb} \int \cos \phi d\phi$$

or

$$\Delta p = \frac{Z_1 Z_2 e^2}{vb} (\sin \phi_2 - \sin \phi_1). \quad (2.14)$$

From Fig. 2.7,  $\phi_1 = -\phi_0$  and  $\phi_2 = +\phi_0$ , where  $2\phi_0 + \theta = 180^\circ$ . Then  $\sin \phi_2 - \sin \phi_1 = 2 \sin(90^\circ - \frac{1}{2}\theta)$ . Combining Eqs. 2.12 and 2.14 for  $\Delta p$ , we have

$$\Delta p = 2M_1 v \sin \frac{\theta}{2} = \frac{Z_1 Z_2 e^2}{vb} 2 \cos \frac{\theta}{2}. \quad (2.15a)$$

This gives the relationship between the impact parameter  $b$  and the scattering angle:

$$b = \frac{Z_1 Z_2 e^2}{M_1 v^2} \cot \frac{\theta}{2} = \frac{Z_1 Z_2 e^2}{2E} \cot \frac{\theta}{2}. \quad (2.15b)$$

From Eq. 2.10, the scattering cross section can be expressed as

$$\sigma(\theta) = \frac{-b}{\sin \theta} \frac{db}{d\theta}, \quad (2.16)$$

and from the geometrical relations  $\sin \theta = 2 \sin(\theta/2) \cos(\theta/2)$  and  $d \cot(\theta/2) = -\frac{1}{2} d\theta / \sin^2(\theta/2)$ ,

$$\sigma(\theta) = \left( \frac{Z_1 Z_2 e^2}{4E} \right)^2 \frac{1}{\sin^4 \theta/2}. \quad (2.17)$$

This is the scattering cross section originally derived by Rutherford. The experiments by Geiger and Marsden in 1911–1913 verified the predictions that the amount of scattering was proportional to  $(\sin^4 \theta/2)^{-1}$  and  $E^{-2}$ . In addition, they found that the number of elementary charges in the center of the atom is equal to roughly half the atomic weight. This observation introduced the concept of the atomic number of an element, which describes the positive charge carried by the nucleus of the atom. The very experiments that gave rise to the picture of an atom as a positively charged nucleus surrounded by orbiting electrons has now evolved into an important materials analysis technique.

For Coulomb scattering, the distance of closest approach,  $d$ , of the projectile to the scattering atom is given by equating the incident kinetic energy,  $E$ , to the potential energy at  $d$ :

$$d = \frac{Z_1 Z_2 e^2}{E}. \quad (2.18)$$

The scattering cross section can be written as  $\sigma(\theta) = (d/4)^2 / \sin^4 \theta/2$ , which for  $180^\circ$  scattering gives  $\sigma(180^\circ) = (d/4)^2$ . For 2 MeV  $\text{He}^+$  ions ( $Z_1 = 2$ ) incident on Ag ( $Z_2 = 47$ ),

$$d = \frac{(2)(47) \cdot (1.44 \text{ eV nm})}{2 \times 10^6 \text{ eV}} = 6.8 \times 10^{-5} \text{ nm},$$

a value much smaller than the Bohr radius  $a_0 = \hbar^2/m_e e^2 = 0.053 \text{ nm}$  and the  $K$ -shell radius of Ag,  $a_0/47 \cong 10^{-3} \text{ nm}$ . Thus the use of an unscreened cross section is justified. The cross section for scattering to  $180^\circ$  is

$$\sigma(\theta) = (6.8 \times 10^{-5} \text{ nm})^2 / 16 = 2.89 \times 10^{-10} \text{ nm}^2,$$

a value of  $2.89 \times 10^{-24} \text{ cm}^2$  or 2.89 barns, where the barn  $= 10^{-24} \text{ cm}^2$ .

## 2.6 Scattering Cross Section: Two-Body

In the previous section, we used central forces in which the energy of the incident particle was unchanged through its trajectory. From the kinematics (Section 2.2), we know that the target atom recoils from its initial position, and hence the incident particle loses energy in the collision. The scattering is elastic in that the total kinetic energy of the particles is conserved. Therefore, the change in energy of the scattered particle can be appreciable; for  $\theta = 180^\circ$  and  ${}^4\text{He}^+ (M_1 = 4)$  scattering from Si ( $M_2 = 28$ ), the kinematic factor  $K = (24/32)^2 = 0.56$  indicates that nearly one-half the energy is lost by the incident particle. In this section, we evaluate the scattering cross section while including this recoil effect. The derivation of the center of mass to laboratory transformation is given in Section 2.10.

The scattering cross section (Eq. 2.17) was based on the one-body problem of the scattering of a particle by a fixed center of force. However, the second particle is not fixed but recoils from its initial position as a result of the scattering. In general, the two-body central force problem can be reduced to a one-body problem by replacing

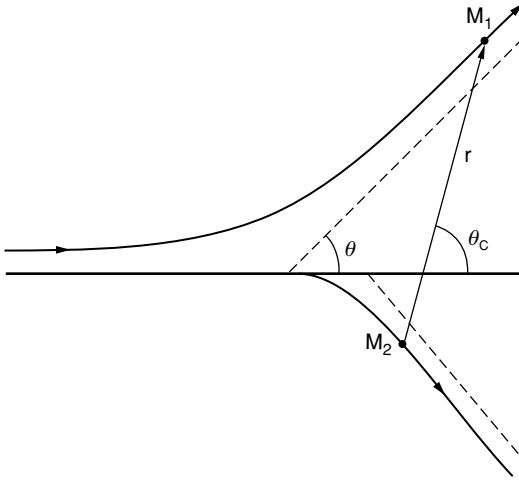


FIGURE 2.9. Scattering of two particles as viewed in the laboratory system, showing the laboratory scattering angle  $\theta$  and the center of mass scattering angle  $\theta_c$ .

$M_1$  by the reduced mass  $\mu = M_1 M_2 / (M_1 + M_2)$ . The matter is not quite that simple as indicated in Fig. 2.9. The laboratory scattering angle  $\theta$  differs from the angle  $\theta_c$  calculated from the equivalent, reduced-mass, one-body problem. The two angles would only be the same if the second remains stationary during the scattering (i.e.,  $M_2 \gg M_1$ ).

The relation between the scattering angles is

$$\tan \theta = \frac{\sin \theta_c}{\cos \theta_c + M_1/M_2},$$

derived in Eq. 2.24. The transformation gives

$$\sigma(\theta) = \left( \frac{Z_1 Z_2 e^2}{4E} \right)^2 \frac{4}{\sin^4 \theta} \frac{\left( \{1 - [(M_1/M_2) \sin \theta]^2\}^{1/2} + \cos \theta \right)^2}{\{1 - [(M_1/M_2) \sin \theta]^2\}^{1/2}}, \quad (2.19)$$

which can be expanded for  $M_1 \ll M_2$  in a power series to give

$$\sigma(\theta) = \left( \frac{Z_1 Z_2 e^2}{4E} \right)^2 \left[ \sin^{-4} \frac{\theta}{2} - 2 \left( \frac{M_1}{M_2} \right)^2 + \dots \right], \quad (2.20)$$

where the first term omitted is of the order of  $(M_1/M_2)^4$ . It is clear that the leading term gives the cross section of Eq. 2.17, and that the corrections are generally small. For  $\text{He}^+$  ( $M_1 = 4$ ) incident on Si ( $M_2 = 28$ ),  $2(M_1/M_2)^2 \cong 4\%$ , even though appreciable energy is lost in the collision. For accurate quantitative analysis, this correction should be included, as the correction can be appreciable for scattering from light atoms such as carbon or oxygen. Cross section values given in Appendix 2 are based on Eq. 2.19. A summary of scattering relations and cross section formulae are given in Table 3.1.

## 2.7 Deviations from Rutherford Scattering at Low and High Energy

The derivation of the Rutherford scattering cross section is based on a Coulomb interaction potential  $V(r)$  between the particle  $Z_1$  and target atom  $Z_2$ . This assumes that the particle velocity is sufficiently large so that the particle penetrates well inside the orbitals of the atomic electrons. Then scattering is due to the repulsion of two positively charged nuclei of atomic number  $Z_1$  and  $Z_2$ . At larger impact parameters found in small-angle scattering of MeV He ions or low-energy, heavy ion collisions (discussed in Chapter 4), the incident particle does not completely penetrate through the electron shells, and hence the innermost electrons screen the charge of the target atom.

We can estimate the energy where these electron screening effects become important. For the Coulomb potential to be valid for backscattering, we require that the distance of closest approach  $d$  be smaller than the  $K$ -shell electron radius, which can be estimated as  $a_0/Z_2$ , where  $a_0 = 0.053$  nm, the Bohr radius. Using Eq. 2.18 for the distance of closest approach  $d$ , the requirement for  $d$  less than the radius sets a lower limit on the energy of the analysis beam and requires that

$$E > Z_1 Z_2^2 \frac{e^2}{a_0}.$$

This energy value corresponds to  $\sim 10$  keV for  $\text{He}^+$  scattering from silicon and  $\sim 340$  keV for  $\text{He}^+$  scattering from Au ( $Z_2 = 79$ ). However, deviations from the Rutherford scattering cross section occur at energies greater than the screening limit estimate given above, as part of the trajectory is always outside of the electron cloud.

In Rutherford-backscattering analysis of solids, the influence of screening can be treated to the first order (Chu et al., 1978) by using a screened Coulomb cross section  $\sigma_{\text{sc}}$  obtained by multiplying the scattering cross section  $\sigma(\theta)$  given in Eqs. 2.19 and 2.20 by a correction factor  $F$ ,

$$\sigma_{\text{sc}} = \sigma(\theta)F, \quad (2.21)$$

where  $F = (1 - 0.049 Z_1 Z_2^{4/3}/E)$  and  $E$  is given in keV. Values of the correction factor are given in Fig. 2.10. With 1 MeV  $^4\text{He}^+$  ions incident on Au atoms, the correction factor corresponds to only 3%. Consequently, for analysis with 2 MeV  $^4\text{He}^+$  ions, the screening correction can be neglected for most target elements. At lower analysis energies or with heavier incident ions, screening effects may be important.

At higher energies and small impact parameter values, there can be large departures from the Rutherford scattering cross section due to the interaction of the incident particle with the nucleus of the target atom. Deviations from Rutherford scattering due to nuclear interactions will become important when the distance of closest approach of the projectile-nucleus system becomes comparable to  $R$ , the nuclear radius. Although the size of the nucleus is not a uniquely defined quantity, early experiments with alpha-particle scattering indicated that the nuclear radius could be expressed as

$$R = R_0 A^{1/3}, \quad (2.22)$$

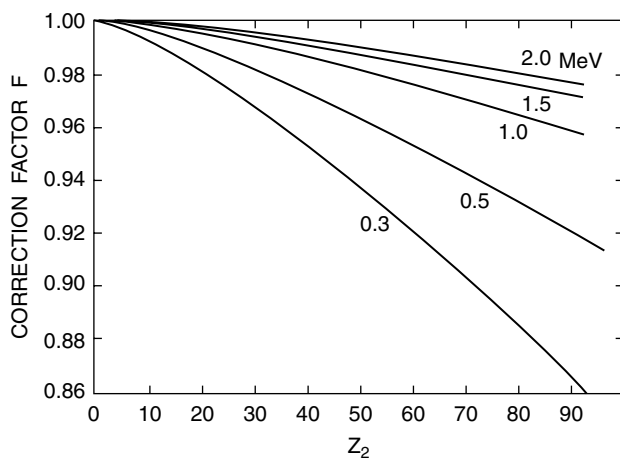


FIGURE 2.10. Correction factor  $F$ , which describes the deviation from pure Rutherford scattering due to electron screening for  $\text{He}^+$  scattering from the atoms  $Z_2$ , at a variety of incident kinetic energies. [Courtesy of John Davies]

where  $A$  is the mass number and  $R_0 \cong 1.4 \times 10^{-13}$  cm. The radius has values from a few times  $10^{-13}$  cm in light nuclei to about  $10^{-12}$  cm in heavy nuclei. When the distance of closest approach  $d$  becomes comparable with the nuclear radius, one should expect deviations from the Rutherford scattering. From Eqs. 2.18 and 2.22, the energy where  $R = d$  is

$$E = \frac{Z_1 Z_2 e^2}{R_0 A^{1/3}}.$$

For  $^4\text{He}^+$  ions incident on silicon, this energy is about 9.6 MeV. Consequently, nuclear reactions and strong deviations from Rutherford scattering should not play a role in backscattering analyses at energies of a few MeV.

One of the exceptions to the estimate given above is the strong increase (resonance) in the scattering cross section at 3.04 MeV for  $^4\text{He}^+$  ions incident on  $^{16}\text{O}$ , as shown in Fig. 2.11. This reaction can be used to increase the sensitivity for the detection of oxygen. Indeed, many nuclear reactions are useful for element detection, as described in Chapter 13.

## 2.8 Low-Energy Ion Scattering

Whereas MeV ions can penetrate on the order of microns into a solid, low-energy ions ( $\sim\text{keV}$ ) scatter almost predominantly from the surface layer and are of considerable use for *first monolayer analysis*. In low-energy scattering, incident ions are scattered, via binary events, from the atomic constituents at the surface and are detected by an electrostatic analyzer (Fig. 2.12). Such an analyzer detects only charged

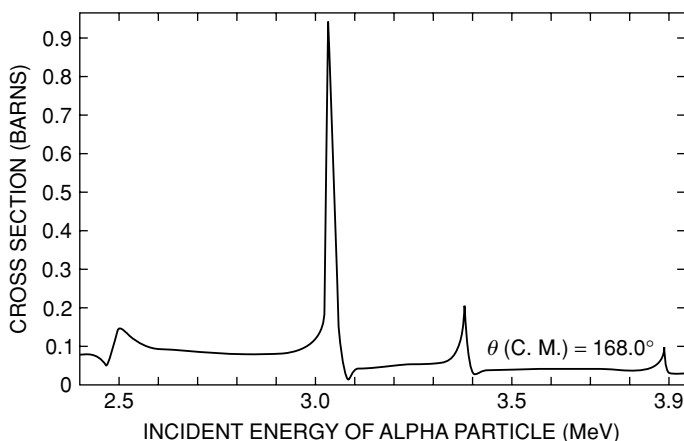


FIGURE 2.11. Cross section as a function of energy for elastic scattering of  $^4\text{He}^+$  from oxygen. The curve shows the anomalous cross section dependence near 3.0 MeV. For reference, the Rutherford cross section 3.0 MeV is  $\sim 0.037$  barns.

particles, and in this energy range ( $\cong 1$  keV), particles that penetrate beyond a monolayer emerge nearly always as neutral atoms. Thus this experimental sensitivity to only charged particles further enhances the surface sensitivity of low-energy ion scattering. The main reasons for the high surface sensitivity of low-energy ion scattering is the charge selectivity of the electrostatic analyzer as well as the very large cross section for scattering.

The kinematic relations between energy and mass given in Eqs. 2.5 and 2.7 remain unchanged for the 1 keV regime. Mass resolution is determined as before by the energy resolution of the electrostatic detector. The shape of the energy spectrum is, however, considerably different than that with MeV scattering. The spectrum consists of a series of peaks corresponding to the atomic masses of the atoms in the surface layer.

Quantitative analysis in this regime is not straightforward for two primary reasons: (1) uncertainty in the absolute scattering cross section and (2) lack of knowledge of the probability of neutralization of the surface scattered particle. The latter factor is minimized by use of projectiles with a low neutralization probability and use of detection techniques that are insensitive to the charge state of the scattered ion.

Estimates of the scattering cross section are made using screened Coulomb potentials, as discussed in the previous section. The importance of the screening correction is shown in Fig. 2.13, which compares the pure Rutherford scattering cross section to two different forms of the screened Coulomb potential. As mentioned in the previous section, the screening correction for  $\sim 1$  MeV He ions is only a few percent (for  $\text{He}^+$  on Au) but is 2–3 orders of magnitude at  $\sim 1$  keV. Quantitative analysis is possible if the scattering potential is known. The largest uncertainty in low-energy ion scattering is not associated with the potential but with the neutralization probability, of relevance when charge sensitive detectors are used.

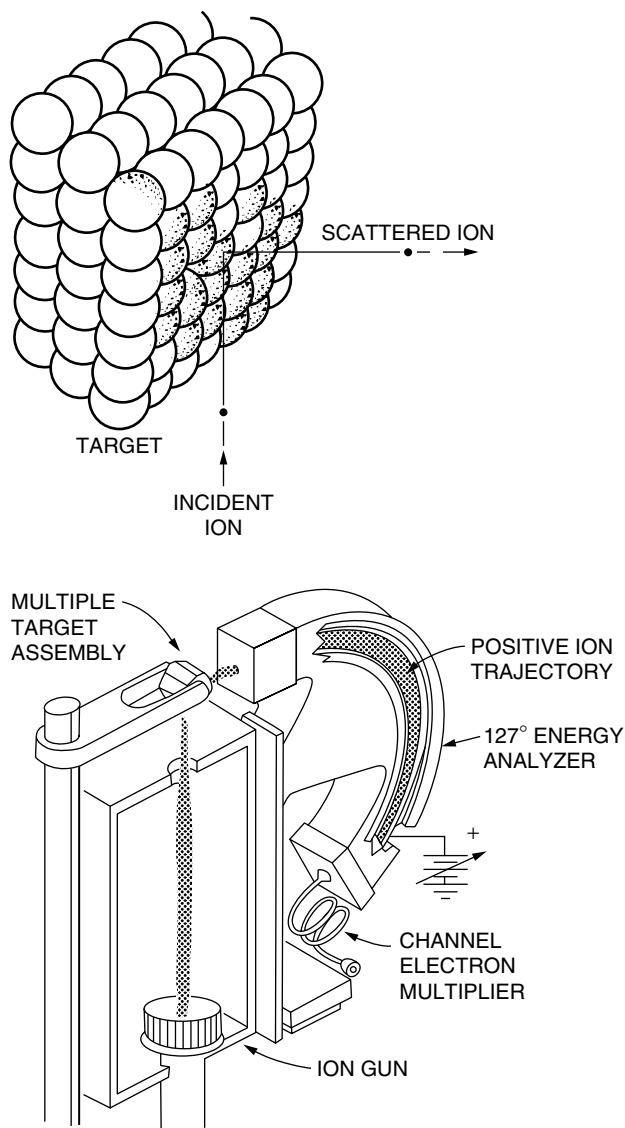


FIGURE 2.12. Schematic of self-contained electrostatic analyzer system used in low-energy ion scattering. The ion source provides a beam of low-energy ions that are scattered (to  $90^\circ$ ) from samples held on a multiple target assembly and analyzed in a  $127^\circ$  electrostatic energy analyzer.

Low-energy spectra for  $^3\text{He}$  and  $^{20}\text{Ne}$  ions scattered from an Fe–Re–Mo alloy are shown in Fig. 2.14. The improved mass resolution associated with heavier mass projectiles is used to clearly distinguish the Mo from the Re. This technique is used in studies of surface segregation, where relative changes in the surface composition can readily be obtained.

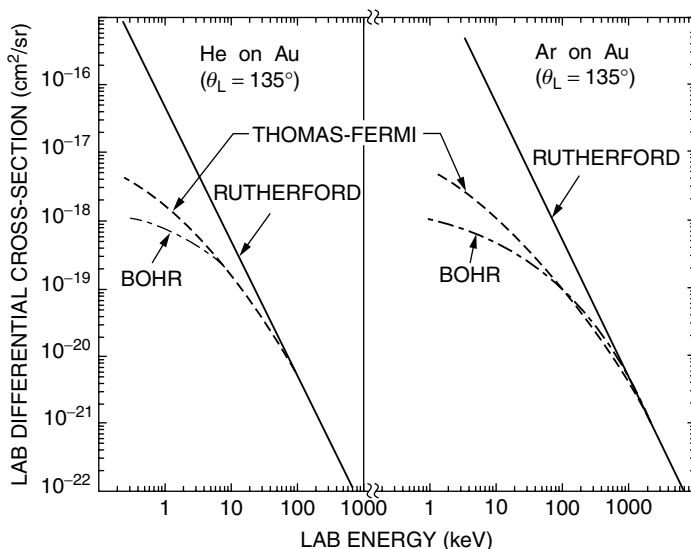


FIGURE 2.13. Energy dependence of the Rutherford, Thomas–Fermi, and Bohr cross sections for a laboratory scattering angle of  $135^\circ$ . The Thomas–Fermi and Bohr potentials are two common approximations to a screened Coulomb potential: (a)  $\text{He}^+$  on Au and (b) Ar on Au. From J.M. Poate and T.M. Buck, *Experimental Methods in Catalytic Research*, Vol. 3. [Academic Press, New York, 1976, vol. 3.]

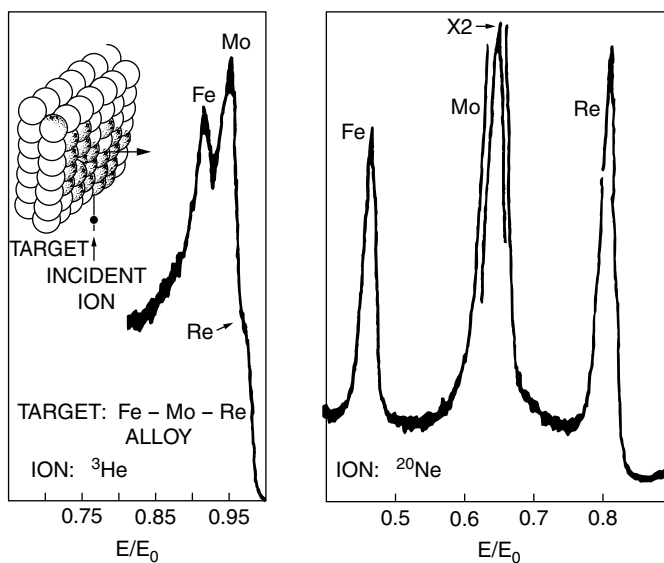


FIGURE 2.14. Energy spectra for  $^3\text{He}^+$  scattering and  $^{20}\text{Ne}$  scattering from a Fe–Mo–Re alloy. Incident energy was 1.5 keV. [From J.T. McKinney and J.A. Leys, *8<sup>th</sup> National Conference on Electron Probe Analysis*, New Orleans, LA, 1973.]



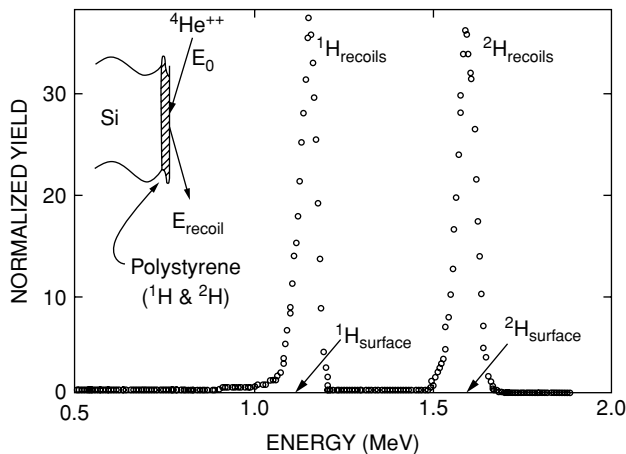


FIGURE 2.15. The forward recoil structures of  $^1\text{H}$  and  $^2\text{H}$  (deuterium) from 3.0 MeV  $^4\text{He}^+$  ions incident on a thin ( $\approx 200$  nm) polystyrene film on silicon. The detector is placed so that the recoil angle  $\phi = 30^\circ$ . A mylar film 10 micron ( $\mu\text{m}$ ) thick mylar film is mounted in front of the detector.

## 2.9 Forward Recoil Spectrometry

In elastic collisions, particles are not scattered in a backward direction when the mass of the incident particle is equal to or greater than that of the target atom. The incident energy is transferred primarily to the lighter target atom in a recoil collision (Eq. 2.7). The energy of the recoils can be measured by placing the target at a glancing angle (typically  $15^\circ$ ) with respect to the beam direction and by moving the detector to a forward angle ( $\theta = 30^\circ$ ), as shown in the inset of Fig. 2.15. This scattering geometry allows detection of hydrogen and deuterium at concentration levels of 0.1 atomic percent and surface coverages of less than a monolayer.

The spectrum for  $^1\text{H}$  and  $^2\text{H}$  (deuteron) recoils from a thin polystyrene target are shown in Fig. 2.15. The recoil energy from 3.0 MeV  $^4\text{He}^+$  irradiation and recoil angle  $\phi$  of  $30^\circ$  can be calculated from Eq. 2.7' to be 1.44 MeV and 2.00 MeV for  $^1\text{H}$  and  $^2\text{H}$ , respectively. Since  $^2\text{H}$  nuclei recoiling from the surface receive a higher fraction ( $\sim 2/3$ ) of the incident energy  $E_0$  than do  $^1\text{H}$  nuclei ( $\sim 1/2$ ), the peaks in the spectrum are well separated in energy. The energies of the detected recoils are shifted to lower values than the calculated position due to the energy loss in the mylar film placed in front of the detector to block out  $\text{He}^+$  ions scattered from the substrate.

The application of forward recoil spectrometry to determine hydrogen and deuterium depth profiles is discussed in Chapter 3. The forward recoil geometry can also be used to detect other light-mass species as long as heavy-mass analysis particles are used.

## 2.10 Center of Mass to Laboratory Transformation

The derivation of the Rutherford cross section assumes a fixed center of force. In practice, the scattering involves two bodies, neither of which is fixed. In general, any

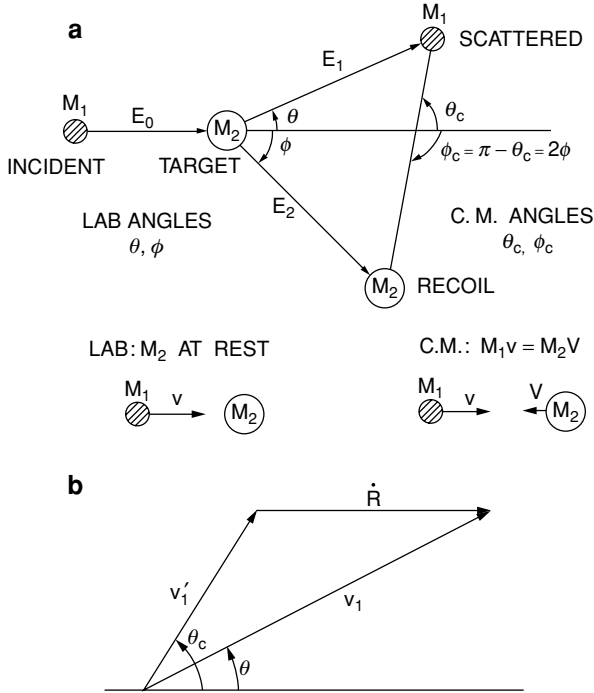


FIGURE 2.16. (a) The relationship between the scattering angles in the laboratory system, namely,  $\theta$  and  $\phi$ , and the scattering angles in the center of the mass system,  $\theta_c$ ,  $\phi_c$ . (b) Vector diagram illustrating the relationship between the velocity of particle 1 in the laboratory system,  $\mathbf{v}_1$ , and the velocity in the center of mass system,  $\mathbf{v}'_1$ .

two-body central force problem can be reduced to a one-body problem. However, since actual measurements are done in the laboratory, one must be aware of the appropriate transformation. The transformation equations yield finite and important *corrections* that must be incorporated in careful analytical work. These corrections are most important when the mass of the projectile,  $M_1$ , becomes comparable to the mass of the target  $M_2$ . Under these conditions, the recoil effects (nonfixed scattering center) become largest.

The relationship between the scattering angles in the laboratory system, namely,  $\theta$  and  $\phi$ , and the angles in the center of mass (CM) system are illustrated in Fig. 2.16a. The first step is to determine an analytical relation between the scattering angles in the two systems.

We use the following notation:  $\mathbf{r}_1$  and  $\mathbf{v}_1$  are the position and velocity vectors of the incident particle in the laboratory system;  $\mathbf{r}'_1$  and  $\mathbf{v}'_1$  are the position and velocity vectors of the incident particle in the center-of-mass system; and  $\mathbf{R}$  and  $\dot{\mathbf{R}}$  are the position and velocity vectors of the center of mass in the laboratory system.

By definition,

$$\mathbf{r}_1 = \mathbf{R} + \mathbf{r}'_1,$$

so

$$\mathbf{v}_1 = \dot{\mathbf{R}} + \mathbf{v}'_1.$$

The geometrical relationship between vectors and scattering angles shown in Fig. 2.16b indicates the relation

$$\tan \theta = \frac{v_1' \sin \theta_c}{v_1' \cos \theta_c + |\dot{\mathbf{R}}|}. \quad (2.23)$$

The definition of the center-of-mass vector,  $\mathbf{R}$ , is

$$(M_1 + M_2)\mathbf{R} = M_1\mathbf{r}_1 + M_2\mathbf{r}_2,$$

so that

$$(M_1 + M_2)\dot{\mathbf{R}} = M_1\dot{\mathbf{r}}_1 + M_2\dot{\mathbf{r}}_2,$$

where  $M_2, \mathbf{r}_2$  refers to the target atom. From the vector diagram,

$$\mathbf{v}_1' = \mathbf{v}_1 - \dot{\mathbf{R}},$$

or

$$\mathbf{v}_1' = \frac{M_2}{M_1 + M_2} (\dot{\mathbf{r}}_1 - \dot{\mathbf{r}}_2).$$

Since the system is conservative, the relative velocity,  $\dot{\mathbf{r}}_1 - \dot{\mathbf{r}}_2$ , is the same before and after the collision. Initially,  $\dot{\mathbf{r}}_2 = 0$ , so

$$v_1' = \frac{M_2}{M_1 + M_2} v,$$

where  $v$  is the initial velocity of the particle. The constant velocity of the CM can also be derived from the definition:

$$(M_1 + M_2)\dot{\mathbf{R}} = M_1\mathbf{v}.$$

Substituting the relations for  $\dot{\mathbf{R}}$  and  $v_1'$  in Eq. 2.23, we have

$$\tan \theta = \frac{\sin \theta_c}{\cos \theta_c + \frac{M_1}{M_2}}. \quad (2.24)$$

When  $M_1 \ll M_2$ , the angles in the two systems are approximately equal; the massive scatterer  $M_2$  suffers little recoil. A useful form of Eq. 2.24 is written as

$$\cot \theta = \cot \theta_c + x \csc \theta_c,$$

where  $x = M_1/M_2$ . This can be rearranged to yield

$$\cot \theta - \cot \theta_c = x \csc \theta_c,$$

or

$$\sin \theta_c \cos \theta - \cos \theta_c \sin \theta = x \sin \theta$$

so that

$$\sin(\theta_c - \theta) = x \sin \theta. \quad (2.25)$$

For simplicity, we let  $\xi = \theta_c - \theta$ . From Eq. 2.25, we have

$$\cos \xi d\xi = x \cos \theta d\theta$$

and

$$\frac{d\xi}{d\theta} = \frac{d\theta_c}{d\theta} - 1 = \frac{x \cos \theta}{\cos \xi},$$

or

$$\frac{d\theta_c}{d\theta} = \frac{\sin \theta_c}{\sin \theta \cos \xi}.$$

Then

$$\frac{d\sigma}{d\Omega} = \left( \frac{Z_1 Z_2 e^2}{2E} \right)^2 \left[ \frac{(1+x) \sin \theta_c}{2 \sin \theta \sin^2 \theta_c / 2} \right]^2 / \cos \xi,$$

where  $E$ , the energy in lab coordinates, is given by

$$E = E_c(1+x).$$

It is useful to derive an expression for the cross section simply in terms of  $\theta$  and  $x$ . We make use of the fact that

$$\begin{aligned} 1+x &= (\sin \xi + \sin \theta) / \sin \theta, \\ \sin(\theta_c/2) \sin^2(\theta_c/2) &= \cot(\theta_c/2), \\ \frac{\sin \theta + \sin \xi}{\cos \theta + \cos \xi} &= \tan \frac{\theta_c}{2}, \end{aligned}$$

so that

$$\frac{(1+x) \sin \xi_c}{2 \sin^2(\theta_c/2)} = \frac{\cos \theta + \cos \xi}{\sin \theta}$$

and

$$\frac{d\sigma}{d\Omega} = \left( \frac{Z_1 Z_2 e^2}{2E} \right)^2 \frac{(\cos \theta + \cos \xi)^2}{\sin^4 \theta \cos \xi}.$$

Noting that  $\cos \xi = (1 - \sin^2 \xi)^{1/2} = (1 - x^2 \sin^2 \theta)^{1/2}$ , we obtain

$$\frac{d\sigma}{d\Omega} = \left( \frac{Z_1 Z_2 e^2}{2E} \right)^2 \frac{[\cos \theta + (1 - x^2 \sin^2 \theta)^{1/2}]^2}{\sin^4 \theta (1 - x^2 \sin^2 \theta)^{1/2}}, \quad (2.26)$$

which is the form given in Eq. 2.19.

## Problems

- 2.1.  ${}^4\text{He}^{++}$  particles are scattered from a thin foil of an elemental material with atomic number  $Z_1$ , mass density  $\rho_1$ , number  $A_1$ , and thickness  $t_1$ , and are observed at some fixed angle  $\theta$ . The first foil is replaced with a second one ( $Z_2, \rho_2, A_2, t_2$ ). What is the ratio of the number of particles observed at  $\theta$  for the first and second foils?
- 2.2. A beam of 2 MeV helium ions is incident on a silver foil  $10^{-6}$  cm thick and undergoes Coulomb scattering in accordance with the Rutherford formula.

- (a) What is the distance of closest approach?
- (b) Find the impact parameter for  $\text{He}^+$  ions scattered through  $90^\circ$ .
- (c) What fraction of the incident 2 MeV  $\text{He}^+$  ions will be backscattered (i.e.,  $\theta > 90^\circ$ )?

The density of silver is  $10.50 \text{ g/cm}^3$ , and its atomic weight is  $107.88 \text{ g mol}^{-1}$ . [Hint: The integrated cross section for scattering through angles  $0^\circ$  to  $90^\circ$  is  $\int_0^{\pi/2} d\sigma$ .]

- 2.3. An  $\alpha$  particle,  $^4\text{He}^+$ , makes a head-on collision with (a) a gold nucleus, (b) a carbon nucleus, (c) an  $\alpha$  particle, and (d) an electron, each initially at rest. What fraction of the  $\alpha$  particle's initial kinetic energy is transferred to the struck particle in each instance?
- 2.4. (a) Using the formula for the Rutherford scattering cross section in center-of-mass coordinates (CM) and the relations for the recoil energy (Eq. 2.7), and noting that  $\phi = \pi/2 - \theta_c/2$  (Fig. 2.16), calculate an expression for  $d\sigma/dE_2$ , the cross section for transferring an energy  $E_2$  to a nucleus. Hint:

$$\frac{d\sigma}{d\theta_c} \frac{d\theta_c}{dE_2} = \frac{d\sigma}{dE_2}.$$

- (b) Using the result of part (a), integrate  $d\sigma/dE_2$  from  $E_{\min}$  to  $E_{\max}$  to find the *total* cross section for transferring an energy greater than  $E_{\min}$ .
- (c) Evaluate the result of part (b) in  $\text{cm}^2$  for the case of 1.0 MeV He ions bombarding Si. Use  $E_{\min} = 14 \text{ eV}$ , the displacement energy of a Si atom bound in an Si lattice. Compare this cross section to  $\sigma_{\text{Ruth}}(\theta = 180^\circ)$ .
- (d) Use the result of (c) to calculate the fraction of atoms displaced (i.e., undergoing an energy transfer greater than 14 eV) for 1  $\mu\text{C}$  of  $\text{He}^+$  ions incident on a target where the  $\text{He}^+$  beam diameter = 1 mm. This result is only a lower limit to the displacements, since we have ignored displacements due to recoiling Si atoms.
- 2.5. A carbon film is known to contain surface contaminants of Au, Ag, and Si. Sketch the backscattering spectrum, indicating the energies of the various peaks and their relative heights.
- 2.6. An accelerator produces an  $\text{He}^+$  ion current of 50 nA at 1.0 MeV. Using a  $1 \text{ cm}^2$  detector 5 cm from the target at a scattering angle of  $170^\circ$ , determine the smallest amount of Au (atoms/ $\text{cm}^2$ ) that can be detected. Detectability is arbitrarily defined as 100 counts in 1 hr. Under similar conditions, what is the detection limit for oxygen? Compare these limits with the number of atoms/ $\text{cm}^2$  in a monolayer ( $\cong 10^{15} \text{ atoms/cm}^2$ ).
- 2.7. Derive the expression for  $E_2$  (Eq. 2.7'), the energy transferred to the target atom using conservation of energy and momentum relations. Give the expression for  $E_2/E_0$  for  $\theta = 90^\circ$ .
- 2.8. Use the small angle approximation ( $\sin \theta \approx \theta$ ) to show that the scattering cross section can be expressed as  $\sigma(\theta) = (Z_1 Z_2 e^2 / E)^2 (\theta)^{-4}$ . Derive this expression using the impulse approximation in which the force of  $Z_1 Z_2 e^2 / b^2$  acts on the particle for an effective time  $t = l/v$ , where  $l = 2b$ . [Hint: An intermediate step in the derivation is to show that  $b = Z_1 Z_2 e^2 / E\theta$ .]

## *References*

1. W. K. Chu, J. W. Mayer, and M.-A. Nicolet, *Backscattering Spectrometry* (Academic Press, New York, 1978).
2. H. Goldstein, *Classical Mechanics* (Addison-Wesley, Reading, MA, 1959).
3. J. W. Mayer and E. Rimini, *Ion Beam Handbook for Material Analysis* (Academic Press, New York, 1977).
4. F. K. Richtmyer, E. H. Kennard, and T. N. Cooper, *Introduction to Modern Physics*, 6th ed. (McGraw-Hill, New York, 1969).
5. P. A. Tipler, *Modern Physics* (Worth Publishers, New York, 1978).



<http://www.springer.com/978-0-387-29260-1>

Fundamentals of Nanoscale Film Analysis

Alford, T.L.; Feldman, L.C.; Mayer, J.W.

2007, XIV, 336 p., Hardcover

ISBN: 978-0-387-29260-1